View metadata, citation and similar papers at core.ac.uk

brought to you by CORE

provided by Digital Commons @ the Georgia Academy of Science

Georgia Journal of Science

Volume 79 *No. 2 Scholarly Contributions from the Membership and Others*

Article 4

2021

DOUBLE AND TRIPLE BOUNCING SPINNING SOCCER BALL

Shafat A. Mubin
Valdosta State University, smubin@valdosta.edu

Follow this and additional works at: https://digitalcommons.gaacademy.org/gjs

 Part of the Other Physics Commons

Recommended Citation

Mubin, Shafat A. (2021) "DOUBLE AND TRIPLE BOUNCING SPINNING SOCCER BALL," *Georgia Journal of Science*, Vol. 79, No. 2, Article 4.
Available at: https://digitalcommons.gaacademy.org/gjs/vol79/iss2/4

This Research Articles is brought to you for free and open access by Digital Commons @ the Georgia Academy of Science. It has been accepted for inclusion in Georgia Journal of Science by an authorized editor of Digital Commons @ the Georgia Academy of Science.

DOUBLE AND TRIPLE BOUNCING SPINNING SOCCER BALL

Shafat Mubin*
Valdosta State University,
Department of Physics, Astronomy, Geosciences and Engineering Technology
Valdosta, GA 31602
*Corresponding author
Email: smubin@valdosta.edu

ABSTRACT

The trajectories of soccer ball penalty kicks that strike one of the goal-posts while rolling along the surface are simulated and analyzed using conservation of linear and angular momenta. The reflected trajectories upon collisions with the goalpost are calculated and used to determine whether double or triple bounces take place. The analysis is iterated for a range of initial launch speeds, angular velocities, and normal and tangential coefficients of restitution of the goalpost-ball collisions. It is observed that double bounces can take place for almost any combination of the above parameters if the soccer ball strikes the appropriate narrow sectors of the first goalpost. The corresponding parameter ranges and impact areas are considerably more restricted for generating triple bounces. The angular velocity and coefficients of restitution are found to significantly influence the occurrence of multiple bounces.

Keywords Soccer ball dynamics, Penalty kicks, Double bounce, Triple bounce, Goalpost collision, Coefficient of restitution, Conservation of angular momentum

INTRODUCTION

When a penalty kick taken from the designated spot of a standard soccer pitch strikes one of the goalposts, it is significantly more probable for the ball to either enter the goal or bounce away from the goal, than to strike the other goalpost. The significantly less probable outcome of the ball rebounding off the goalpost and striking the other goalpost, i.e. a double bounce penalty, can be produced by appropriate combinations of ball speed, ball spin, impact location and impact surface friction. A geometric analysis of the double bounce penalty kick (Widenhorn, 2016) for a non-spinning soccer ball that undergoes ideal velocity reflection upon striking a goalpost demonstrates that the ball must strike a sliver of the goalpost of width 0.6 mm along the direction of the goal line to produce this occurrence, and the corresponding margin is 0.007 mm for a triple bounce penalty, where the ball hits the second goalpost and goes back to strike the first post. An analytic examination of the same non-spinning case shows analogy with the classic Alhazen's billiard problem (Elkin, 1965), which leads to a quartic equation of the coordinates of impact.

The motivation for Widenhorn's paper was the double bouncing penalty kick during the thrilling MLS match between Portland Timbers and Sporting Kansas City in

2015, which turned out to be a missed match-winner. While Widenhorn's analysis calculates the allowed region of ball-goalpost impact for the penalty kick in concern, it disregards the rotation of the ball clearly visible on video (Youtube link: https://youtu.be/LeTDeRp_ZvI?t=375). By contrast, this paper incorporates more parameters that are encountered during an actual penalty kick and therefore presents an improved study.

In this paper, we expand the above study to incorporate ball speed, ball spin and coefficients of restitution of the goalpost-ball collision to determine double and triple bounce conditions. Similar to the above study, it is assumed that the ball is constrained to travel only on a planar 2D surface and its weight can be ignored. At the same time, this assumption only allows the ball to spin around an axis that passes through the center of the ball perpendicular to the plane along which the ball travels. The wider span of variables introduced by these modifications is analyzed using computational techniques, which generate penalty kick trajectories at different combinations of these variables and identify successful double and triple bounces.

METHOD

The collision in our model is based on the conservation of angular momentum and the impulse provided by the frictional force during contact, as has been studied by Cross (Cross, 2005). The bounce of a spinning ball on a surface is described in terms of the tangential (v_x) and normal (v_y) components of the impact velocity (relative to the impact surface), the angular velocity ω and the normal (e_y) and tangential (e_x) coefficients of restitution (Cross, 2005; Brody, 1984). The two coefficients of restitution are defined as (Cross, 2002):

$$e_y = \frac{v_{y_f}}{v_{y_i}} \tag{1}$$

$$e_x = -\frac{v_{x_f} - R_{ball}\omega_f}{v_{x_i} - R_{ball}\omega_i} \tag{2}$$

where v_{x_i} and v_{y_i} are respectively the tangential and normal components of the impact velocity and v_{x_f} and v_{y_f} are the corresponding components of the rebound velocity of the center-of-mass of the ball, R_{ball} is the radius of the ball, and ω_i and ω_f are angular velocities of the ball (around an axis that passes through its center and is normal to the plane spanned by v_{x_i} and v_{y_i}) before and after impact respectively. The signs of the angular velocities are defined using the direction of rotation and the direction of v_{x_i}: at the instant immediately prior to impact, if the point on the ball that is about to strike the surface has a velocity pointing in the direction opposite to v_{x_i}, i.e. the ball possesses a "topspin", the angular velocity is considered positive; if the above velocity points in the same direction as v_{x_i}, i.e. ball possesses a "backspin", the angular velocity is considered negative (see Appendix). It follows that the point on the ball that strikes the goalpost has

velocities of $(v_{x_i} - R_{ball}\omega_i)$ and $(v_{x_f} - R_{ball}\omega_f)$ immediately before and immediately after impact respectively.

The coefficients e_x and e_y depend on the surface materials in contact, and determine the duration of contact between ball and surface (Cross, 2005). For angles of incidence below 45° of the surface normal, a bounce takes place at $0 < e_y < 1$ and $-1 < e_x < 1$ (Cross, 2005). A combination of $e_y = 1$ and $e_x = -1$ represents a perfectly frictionless collision which conserves both tangential and normal components of the impact velocity. Increasing values of e_x indicate greater friction and "stickier" surfaces, where v_{x_f} has a greater dependence on angular velocities (Cross, 2005; Cross, 2002). The ball moment of inertia around an axis passing through its center is given by $I = \alpha M R_{ball}^2$, where M is the mass of the soccer ball, $R_{ball} = 0.11$ m is the standard soccer ball radius (Laws of the Game, 2019-20) and $\alpha = \frac{2}{3}$ is the moment of inertia coefficient of a spherical shell assuming that the ball shell thickness is negligible. By accounting for conservation of angular momentum for the bounce in terms of the ball moment of inertia, we obtain (Cross, 2002):

$$I\omega_i + MR_{ball}v_{x_i} = I\omega_f + MR_{ball}v_{x_f} \tag{3}$$

and v_{x_f}, v_{y_f} and ω_f can be solved as (Cross, 2005):

$$v_{y_f} = e_y v_{y_i} \tag{4}$$

$$v_{x_f} = v_{x_i}\left[\frac{1-\alpha e_x}{1+\alpha} + \frac{\alpha(1+e_x)}{1+\alpha}\left(\frac{R_{ball}\omega_i}{v_{x_i}}\right)\right] \tag{5}$$

$$\omega_f = \omega_i\left(\frac{\alpha-e_x}{1+\alpha}\right) + \left(\frac{1+e_x}{1+\alpha}\right)\left(\frac{v_{x_i}}{R_{ball}}\right) \tag{6}$$

The above equations imply that coefficients e_x and e_y play a part in determining both the rebound speed and the angular speed after impact. In addition, the rebound velocity components v_{x_f} and v_{y_f} may change disproportionately after impact, which changes the angle of reflection compared to the angle of incidence.

For our analysis, we simulate in Mathematica (Wolfram Mathematica, 2021) the impact of a soccer ball that is launched from the designated penalty spot directed towards a fixed goalpost. The ball skids along the ground, i.e. travels linearly at a constant speed v_1 and constant angular velocity ω_1, and strikes some part of the circular cross-section of the goalpost. It is assumed that only when the ball strikes a goalpost, its velocity and angular velocity are allowed to change. The impact velocity components v_{xi_1} and v_{yi_1} are derived from the impact speed v_1 and incident angle θ_1 (Figure 1) of the ball on the goalpost. The equations above are used to calculate the rebound velocity components (v_{xf_1}, v_{yf_1}) and the rebound angular velocity ω_2, and subsequently used to find the reflected trajectory of the rebounding ball to determine whether the ball strikes the other goalpost, i.e. performs a double bounce. If a double bounce takes place, the incident angle

θ_2 and corresponding incident speed v_2 and velocity components (v_{xi_2}, v_{yi_2}) of the second bounce are calculated, and the resultant rebound trajectory, which has velocity components (v_{xf_2}, v_{yf_2}) and angular velocity ω_3, is similarly calculated to determine whether a triple bounce occurs.

Coordinate System

In our 2D coordinate system, the ball is confined to travel along the ground, which is defined as the xy-plane, and the z-axis passing through the center of the ball represents the axis of rotation. We define the penalty spot as the origin (0,0) and the line joining the penalty spot to the center of the target goalpost as the +x-axis. It is also assumed that the second goalpost lies above the x-axis in the first quadrant. Standard dimensions of a soccer pitch and radii of goalpost and ball are used in this study (Laws of the Game, 2019-20). Using the goalpost radius (R_{post} = 0.05 m), the separation between the goalposts (7.32 m) and the perpendicular distance from the inner edge of the goal line to the penalty spot (11 m), the coordinates of the target goalpost are calculated to be (x_{P_1}, y_{P_1}) = (11.56 m, 0 m) and the second goalpost to be (x_{P_2}, y_{P_2}) = (9.18 m, 7.03 m). The x-axis and the goal line form an angle of Θ_0 = 71.28° (Figure 1).

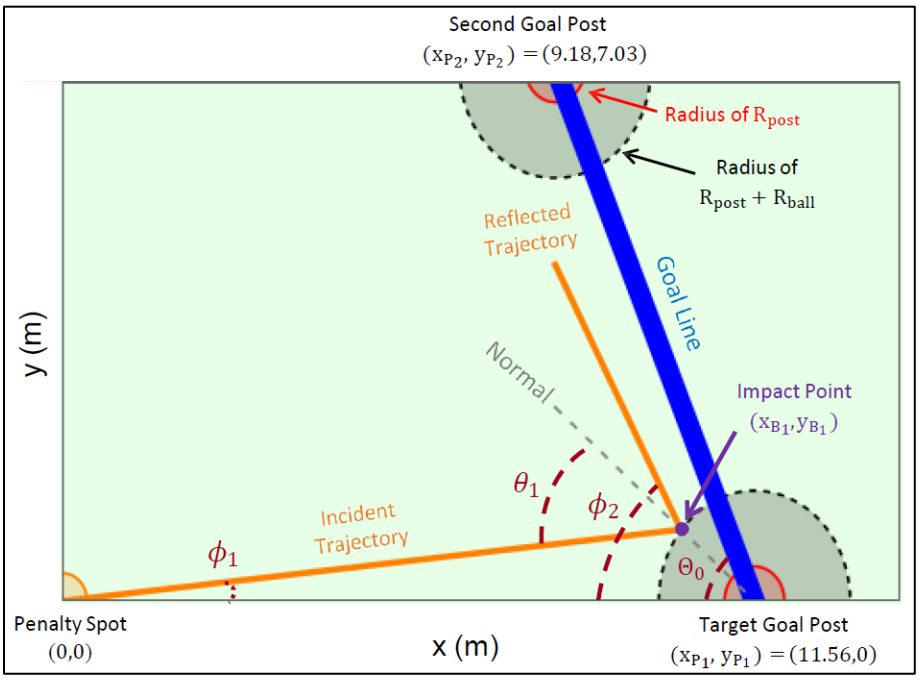

Figure 1. View of setup from above, depicting the coordinate system used to analyze the first bounce and the coordinates of the penalty spot (0,0) m, the first post (11.56,0) m and the second post (9.18,7.03) m. The launch angle ϕ_1, the incident angle θ_1 and the rebound angle ϕ_2 of the first bounce are marked, along with the corresponding incident and reflected trajectories, the impact point (x_{B_1}, y_{B_1}) and the angle Θ_0 = 71.28° between the goal line and the x-axis. The trajectories represent the center of the ball, and accordingly the impact point is shown on the circle with radius $(R_{post} + R_{ball})$.

According to the sign convention for angular velocity described earlier, a clockwise rotation in this setup implies positive angular velocity of the ball and vice-versa, because the ball travels from the penalty spot and strikes the upper half of the target goalpost in Figure 1 (described in the next section). Therefore, a clockwise rotation results in a topspin whereas a counterclockwise rotation results in a backspin when the ball strikes the goalpost. For subsequent double or triple bounces, which involve greater variations in impact region and ball direction, the signs of the angular velocities will be revisited.

First Bounce

The simulated ball is launched towards the target goalpost with an initial speed v_1 and an initial angular velocity ω_1. The center of the ball is directed at a launching angle ϕ_1 measured from the +x-axis, such that the outer surface of the ball collides with some part of the goalpost. The coordinates of the center of the ball at point of impact (x_{B_1}, y_{B_1}) are calculated by equating the center of ball trajectory

$$y_{B_1} = (\tan\phi_1)x_{B_1} \tag{7}$$

with the goalpost circle centered at (x_{P_1}, y_{P_1}) having a combined radius of the ball and goalpost

$$\left(x_{B_1} - x_{P_1}\right)^2 + \left(y_{B_1} - y_{P_1}\right)^2 = \left(R_{ball} + R_{post}\right)^2 \tag{8}$$

to obtain the following solutions for x_{B_1} and y_{B_1}:

$$x_{B_1} = \frac{x_{P_1} - \sqrt{\left(R_{ball}+R_{post}\right)^2(1+\tan^2\phi_1) - \left(x_{P_1}\tan\phi_1\right)^2}}{1+\tan^2\phi_1} \tag{9}$$

$$y_{B_1} = (\tan\phi_1)x_{B_1} \tag{10}$$

The slope of the goalpost at this point of contact is obtained from the derivative of the circle in Eq. (8) evaluated at (x_{B_1}, y_{B_1}):

$$\frac{dy}{dx} = \frac{x_{P_1} - x_{B_1}}{\sqrt{\left(R_{ball}+R_{post}\right)^2 - \left(x_{B_1} - x_{P_1}\right)^2}} \tag{11}$$

The slope of the normal to the goalpost (Figure 1) at this point is therefore the negative reciprocal of the slope above:

$$slope\ of\ normal = -\frac{\sqrt{\left(R_{ball}+R_{post}\right)^2 - \left(x_{B_1} - x_{P_1}\right)^2}}{x_{P_1} - x_{B_1}} \tag{12}$$

The arctan of the above quantity gives the angle between the x-axis and the normal to the goalpost at the impact point (x_{B_1}, y_{B_1}). Then the incident angle θ_1 on the goalpost is geometrically calculated (see Appendix):

$$\theta_1 = \phi_1 - \arctan\left(-\frac{\sqrt{\left(R_{ball}+R_{post}\right)^2-\left(x_{B_1}-x_{P_1}\right)^2}}{x_{P_1}-x_{B_1}}\right) \qquad (13)$$

The impact velocity components are calculated by $v_{xi_1} = v_1 \cos\left(\frac{\pi}{2} - \theta_1\right)$ and $v_{yi_1} = v_1 \sin\left(\frac{\pi}{2} - \theta_1\right)$, and the rebound velocity components v_{xf_1} and v_{yf_1} are obtained from Eq. (4) and Eq. (5). The rebound speed is calculated by $v_2 = \sqrt{\left(v_{xf_1}\right)^2 + \left(v_{yf_1}\right)^2}$ and rebound angle ϕ_2, measured from the x-axis as shown in Figure 1, is given by (see Appendix):

$$\phi_2 = \arcsin\left(\frac{v_{xf_1}}{v_2}\right) - \arctan\left(-\frac{\sqrt{\left(R_{ball}+R_{post}\right)^2-\left(x_{B_1}-x_{P_1}\right)^2}}{x_{P_1}-x_{B_1}}\right) \qquad (14)$$

In the equations above, it is assumed that ϕ_1 is positive (i.e. measured counter-clockwise from +x-axis) and is less than $\frac{\pi}{2}$ (see trial criteria in next paragraph), which leads to a positive θ_1 and positive velocity components (v_{xi_1}, v_{yi_1}). If the ball carries a topspin, i.e. $\omega_1 > 0$, then ϕ_2 must be positive and the ball travels upwards away from the x-axis upon rebound. If the ball carries a sufficiently large backspin, i.e. $\omega_1 < 0$, it is possible to generate a negative ϕ_2, in which case the ball would travel downwards below the x-axis and hence not produce a double bounce. The rebound angular velocity ω_2 is calculated using Eq. (6).

In this study, to simulate typical ball speeds and spins, the initial speed v_1 is varied from 5 to 45 m/s in increments of 2.5 m/s, and the initial angular velocity ω_1 is varied from -45 rad/s to 45 rad/s in increments of 1 rad/s. The launching angle ϕ_1 is varied from 0 to arctan(0.0135) in increments of arctan(0.0001) to locate impact points on the goalpost between the x-axis and the goal line. The coefficients of restitution of collision between ball and goalpost are varied in the ranges $-1 < e_x < 1$ and $0.2 < e_y < 1$ in increments of 0.2. For every combination of parameters above, a simulation trial is performed to determine the trajectories of the ball before and after impact. The direction of the rebound trajectory, defined using ϕ_2, is used to determine whether a double bounce takes place for each trial, as described in the next section.

Double Bounce

A double bounce is considered to occur if ϕ_2 is found to lie between the angles formed by the center of the ball at impact (x_{B_1}, y_{B_1}) and the edges of the second goalpost

circle centered at (x_{P_2}, y_{P_2}) with radius $(R_{ball} + R_{post})$ (Figure 1), which ensures contact between the ball and the second goalpost:

$$\arctan\left[\frac{y_{P_2}-y_{B_1}}{|x_{P_2}-x_{B_1}|+(R_{ball}+R_{post})}\right] \leq \phi_2 \leq \arctan\left[\frac{y_{P_2}-y_{B_1}}{|x_{P_2}-x_{B_1}|-(R_{ball}+R_{post})}\right] \quad (15)$$

The trials that generate ϕ_2's lying within the above range are filtered out and analyzed to determine the incident angle θ_2 and corresponding incident velocity components (v_{xi_2}, v_{yi_2}) of the second bounce. The rebound angular velocity ω_2 derived from the first goalpost impact is used as the initial angular velocity for the second bounce, with a possible sign change (discussed later).

If the system consisting of the two goal posts is transformed to place the center of the first goal post at the origin (0, 0) m and to align the goal line with the x- axis, the same steps used to analyze the first bounce can be reused for the second bounce. In order to perform this transformation, the system is linearly translated by (x_{P_1}, y_{P_1}) and then rotated clockwise through a rotation matrix R:

$$R = \begin{bmatrix} \cos(\pi - \Theta_0) & \sin(\pi - \Theta_0) \\ -\sin(\pi - \Theta_0) & \cos(\pi - \Theta_0) \end{bmatrix} = \begin{bmatrix} -\cos(\Theta_0) & \sin(\Theta_0) \\ -\sin(\Theta_0) & -\cos(\Theta_0) \end{bmatrix} \quad (16)$$

where $(\pi - \Theta_0)$ is the supplementary of the angle between the current x-axis and goal line ($\Theta_0 = 71.28°$).

The coordinates (x_{B_1}, y_{B_1}) are transformed to:

$$\begin{bmatrix} x_{B_1} \\ y_{B_1} \end{bmatrix} = R \begin{bmatrix} x_{B_1} - x_{P_1} \\ y_{B_1} - y_{P_1} \end{bmatrix} \quad (17)$$

Similarly, the center of the second goal post is transformed to $(x_{P_2}, y_{P_2}) \rightarrow (7.42, 0)$ m on the x-axis (Figure 2). The rebound angle ϕ_2 is accordingly transformed by $\phi_2 \rightarrow \Theta_0 - \phi_2$ so that ϕ_2 represents the angle between the transformed x-axis, i.e. the goal line, and the trajectory of the rebounding ball from the first post.

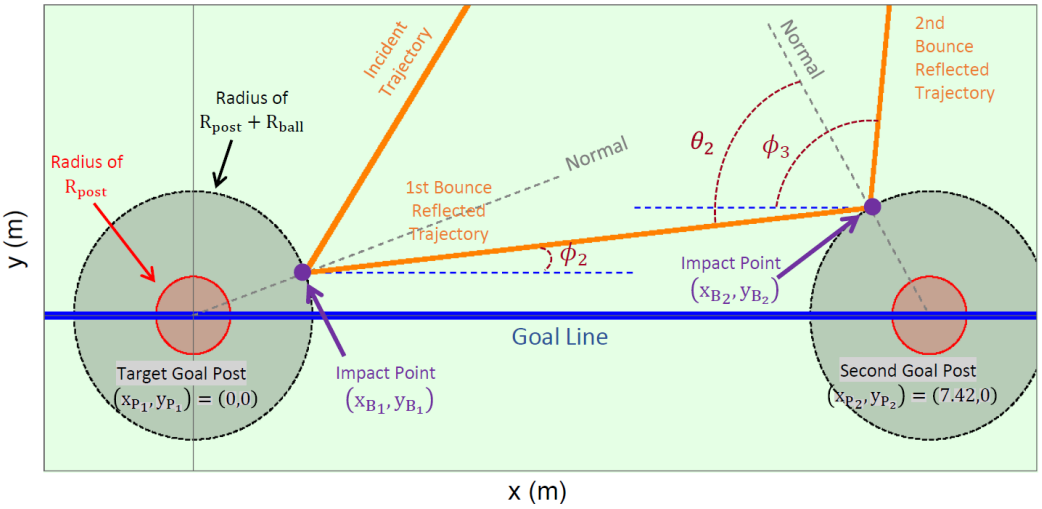

Figure 2. View of transformed coordinate system used to analyze the second bounce. The first goal post is centered at (0,0) m and the second post at (7.42,0) m, while the first bounce impact point (x_{B_1}, y_{B_1}) is transformed accordingly. The rebound angle ϕ_2 is now measured from the new x-axis to the first bounce reflected trajectory. The second bounce incident angle θ_2 and the second bounce rebound angle ϕ_3 are marked in the figure, along with the corresponding incident and reflected trajectories and impact point (x_{B_2}, y_{B_2}) on the second post.

Following from the previous section, the coordinates of the center of the ball at second post impact (x_{B_2}, y_{B_2}) are calculated by equating the center of ball trajectory $y_{B_2} = y_{B_1} + (\tan\phi_2)(x_{B_2} - x_{B_1})$ with the second goalpost circle centered at (x_{P_2}, y_{P_2}) having a combined radius of the ball and goalpost $(x_{B_2} - x_{P_2})^2 + (y_{B_2} - y_{P_2})^2 = (R_{ball} + R_{post})^2$:

$$x_{B_2} = \frac{1}{1+\tan^2\phi_2}\left[x_{P_2} + \tan\phi_2\left(x_{B_1}\tan\phi_2 - y_{B_1} + y_{P_2}\right)\right] - \frac{1}{1+\tan^2\phi_2}\left[\sqrt{(R_{ball} + R_{post})^2(1+\tan^2\phi_2) - \left((x_{B_1} - x_{P_2})\tan\phi_2 - y_{B_1} + y_{P_2}\right)^2}\right] \quad (18)$$

$$y_{B_2} = y_{B_1} + (\tan\phi_2)(x_{B_2} - x_{B_1}) \quad (19)$$

When calculating the incident angle θ_2 on the second post, the slope of the normal at (x_{B_2}, y_{B_2}) is positive if the impact occurs on the lower half of the goal post, i.e. if $y_{B_2} < 0$, and negative on the upper half, i.e. $y_{B_2} > 0$. Therefore, Eq. (13) is modified below to find θ_2:

$$\theta_2 = \phi_2 - sign(y_{B_2})\arctan\left(-\frac{\sqrt{(R_{ball}+R_{post})^2 - (x_{B_2}-x_{P_2})^2}}{x_{P_2}-x_{B_2}}\right) \quad (20)$$

For this second bounce, θ_2 must be negative if the impact occurs on the lower half of the goal post (since ϕ_2 must be negative for such impacts). If ϕ_2 is positive and the all

strikes the upper half of the goalpost while travelling upwards, then θ_2 must be positive. If the ball strikes the upper half of the goal post while travelling downwards at a negative ϕ_2, then θ_2 can be positive or negative depending on impact location and the slope of the normal at that point (Figure 3).

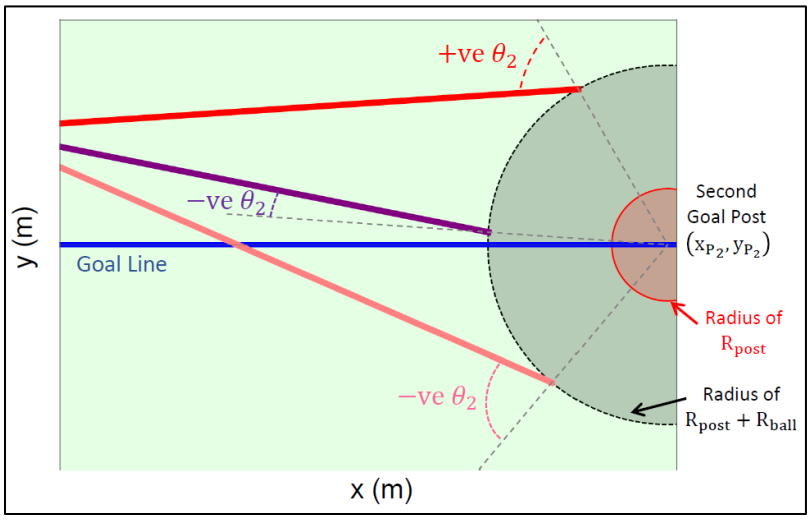

Figure 3. Various ball trajectories (solid lines) incident on the second goal post. If the incident angle θ_2 is traced from the normal to the incident trajectory in a counterclockwise direction, it is considered positive, and vice-versa. For an upward travelling trajectory (with $\phi_2 > 0$), θ_2 must be positive. For a downward travelling trajectory (with $\phi_2 < 0$), θ_2 can be positive, negative or zero depending on the slope of the normal: θ_2 must be negative if the ball strikes the lower half of the goalpost. The normals at impact points are represented by dashed lines.

The impact velocity components $v_{xi_2} = v_2 \cos\left(\frac{\pi}{2} - \theta_2\right)$ and $v_{xi_2} = v_2 \sin\left(\frac{\pi}{2} - \theta_2\right)$ are calculated using the absolute value of θ_2, and Eq. (4), Eq. (5) and Eq. (6) are used to calculate the corresponding rebound velocity components v_{xf_2} and v_{yf_2}, as well as the rebound angular velocity ω_3 (using the same e_x and e_y as for the first bounce). The rebound speed is then obtained from $v_3 = \sqrt{v_{xf_2}^2 + v_{yf_2}^2}$ and the rebound angle ϕ_3, measured from the segment of goal line that lies between the goal posts (Figure 2), is calculated by modifying Eq. (14):

$$\phi_3 = sign(\theta_2)\left[\arcsin\left(\frac{v_{xf_2}}{v_3}\right)\right] - sign(y_{B_2})\left[\arctan\left(-\frac{\sqrt{(R_{ball}+R_{post})^2-(x_{B_2}-x_{P_2})^2}}{x_{P_2}-x_{B_2}}\right)\right] \quad (21)$$

Similar to the determination of double bounces, this rebound angle ϕ_3 is compared with the first goal post coordinates and the combined ball and post radii to filter out trials that undergo triple bounces, as described in the next section.

Triple Bounce

As with double bounces, a triple bounce occurs if ϕ_3 lies between the angles formed by the center of the ball at second impact (x_{B_2}, y_{B_2}) and the edges of the first goalpost circle centered at (x_{P_1}, y_{P_1}) = (0, 0) with radius $(R_{ball} + R_{post})$ (Figure 2):

$$\arctan\left[\frac{y_{P_1}-y_{B_2}-(R_{ball}+R_{post})}{|x_{P_1}-x_{B_2}|}\right] \leq \phi_3 \leq \arctan\left[\frac{y_{P_1}-y_{B_2}+(R_{ball}+R_{post})}{|x_{P_1}-x_{B_2}|}\right] \qquad (23)$$

The trials that generate triple bounces are identified and, similar to the previous sections, the coordinates of the center of the ball at third bounce impacts (x_{B_3}, y_{B_3}) are calculated by equating the center of ball trajectory with the first goalpost circle centered at (0, 0):

$$x_{B_3} = \frac{1}{1+\tan^2(-\phi_3)}\left[\tan(-\phi_3)\left(x_{B_2}\tan(-\phi_3) - y_{B_2}\right)\right] - \frac{1}{1+\tan^2(-\phi_3)}\left[\sqrt{\left(R_{ball}+R_{post}\right)^2(1+\tan^2(-\phi_3)) - \left(x_{B_2}\tan(-\phi_3) - y_{B_2}\right)^2}\right] \qquad (24)$$

$$y_{B_3} = y_{B_2} + (\tan(-\phi_3))(x_{B_3} - x_{B_2}) \qquad (25)$$

where the tan of $(-\phi_3)$ compensates for ϕ_3 being measured between the -x- axis and the ball trajectory (Figure (2)). The results for trials that undergo multiple bounces are analyzed in the following section.

RESULTS AND DISCUSSIONS

Double Bounce

In order to facilitate visual representation of the initial speed v_1, initial angular velocity ω_1 and launch angle ϕ_1 at various values of e_x and e_y studied, a color code designating first bounce impact locations is introduced (Figure (4)). Each 1° sector of the first goalpost impact surface is assigned a specific color that is employed in Figure (5) to designate the impact point of the first bounce. Figure (5) depicts all successful double bounce instances generated within the entire parameter space studied. Each column in Figure (5) represents a specific value of e_y and consists of a stack of v_1 vs ω_1 planes that corresponds to the full range of e_x values analyzed. The color of a point on a plane designates the first bounce impact location that generates a successful double bounce for the particular set of parameters (v_1, ω_1, e_y, e_x) corresponding to that point.

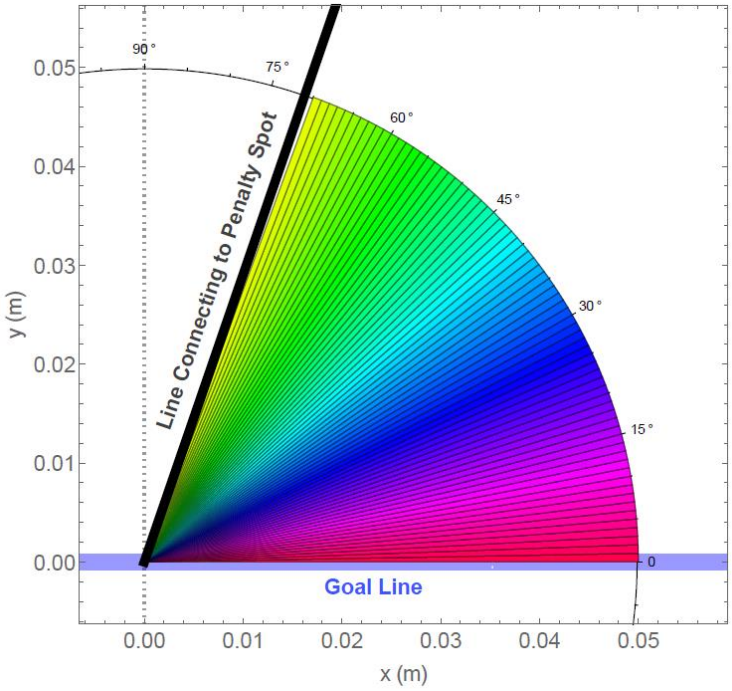

Figure 4. Cross-section of the first goalpost showing the color codes of the first bounce impact surface, which is divided into 1° sectors from the goal line (0°) to the line joining the penalty spot to the goalpost (Θ_0 = 71.28°). Based on its point of impact on this cross-section, every bounce is assigned a color which is then employed in Figure (5) and Figure (9) to represent its first bounce impact location.

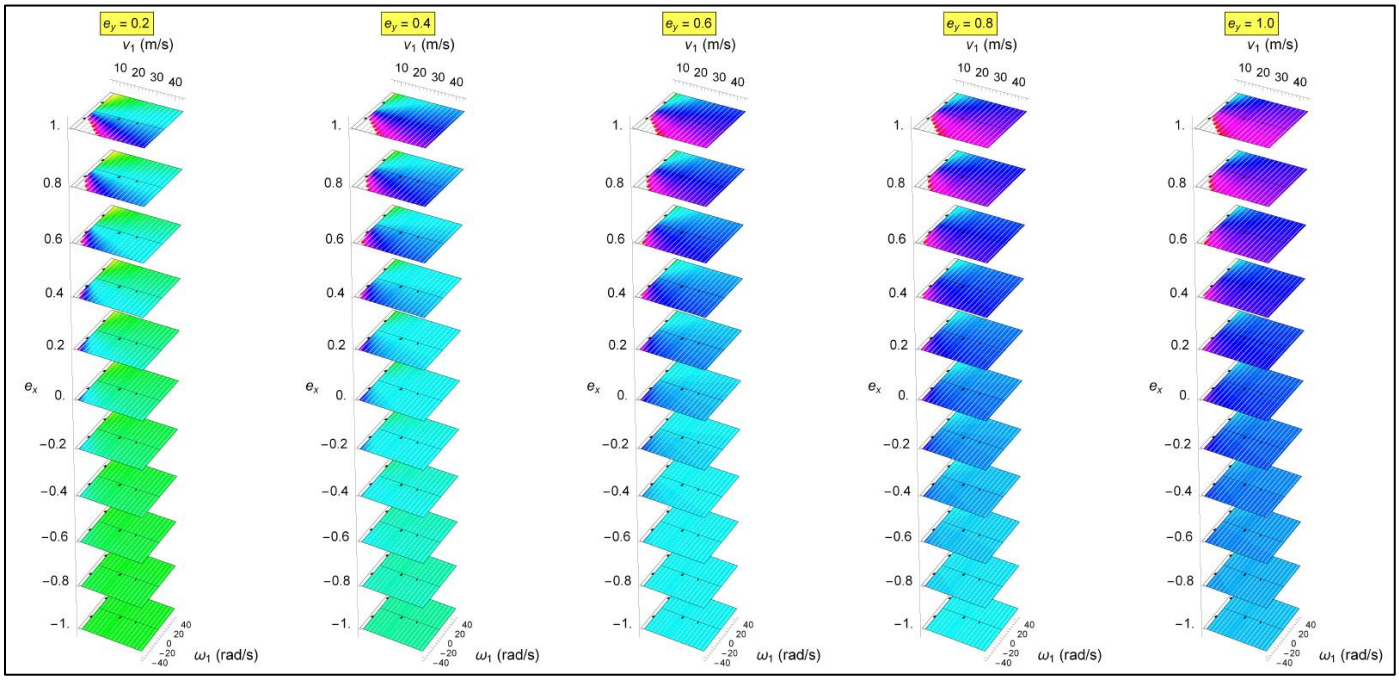

Figure 5. Representation of all data points that produce successful double bounces categorized by e_y (columns), e_x (rows), v_1 (x-axis of planes) and ω_1 (y-axis of planes). Each successful double bounce instance is assigned a color corresponding to the scheme described in Figure (4) to designate its impact point on the

first goalpost during the first bounce (white dots indicate absence of double bounce instances). Altogether, the first bounce impact location and the v_1, ω_1, e_y and e_x of every successful double bounce are captured in this figure.

The bottom-left corner of Figure (5) shows that at the most negative e_x = -1 and the smallest e_y = 0.2, double bounces take place at first bounce impact location at ≈ 50° measured from the x-axis (i.e. colored green in Figure (4)) for all combinations of v_1 and ω_1. Owing to a small e_y, the vertical component of rebound velocity v_{yf_1} drops considerably. Owing to a large negative e_x, the v_{xf_1} does not deviate from v_{xi_1} with zero contribution from angular velocity ω_1, i.e. the goal post surface is frictionless and conserves v_{xi_1}. Altogether, it leads to a larger reflection angle compared to the incident angle irrespective of v_1 or ω_1, and the reflected trajectory from this impact point is directed towards the second goalpost to generate a double bounce.

At increasing values of e_x up the same column, the homogeneity in color fades as we see blue spots appearing at large negative ω_1 values and small v_1 values, implying that impacts at 30° to 45° (i.e. cyan to blue) locations at these combinations produce double bounces. The v_{yf_1} component still diminishes considerably but ω_1 contributes increasingly more to v_{xf_1}. A negative ω_1 contributes to reduce v_{xf_1} and therefore to reduce the reflected angle, whereas a positive ω_1 does the opposite. Towards the top of the column, impact locations at angles of ≈5° (i.e. red) are seen to produce double bounces at large negative ω_1 values which sufficiently alter the reflected trajectory. At the very top plane, a spectrum from low to high angles is observed, blending from small angles (red, violet, blue) at negative ω_1 to large angles (cyan, green, yellow) at positive ω_1. Therefore, for increasing e_x's, an increasingly larger goalpost impact area is available to generate double bounces, but are associated with narrower permitted ranges of v_1 and ω_1. The extreme angles (yellow and red) require small v_1's within narrow ranges of extreme ω_1's for precise reflections, and therefore occupy less space on the v_1 vs ω_1 plane. In addition, there are blank white spots at the corner of large negative ω_1 and small $\backslash v_1$, indicating that these trials did not produce any successful double bounce, primarily because of the disproportionately large backspins deviating the reflected trajectories away from the goal line.

Moving to higher e_y values at the columns on the right, we see increasingly bluer colors at the bottom plane (i.e. e_x =-1) frictionless bounces, indicating that double bounces are generated by first bounce impacts closer to the goal line because of the larger e_y coefficients that contribute to reduce the reflected angle. Going up the columns, the pattern is the same as in the first column - gradual shift to cyan to blue to violet to red impact locations, along with increasing dependence on ω_1 and v_1 as before. At the bottom-right corner of e_y = 1 and e_x = -1, i.e. a collision that conserves both tangential and normal velocity components after collision, reflection and incident angles are equal and double bounce occurs at a blue impact location of angle ≈35°. This impact location agrees with the calculation of Widenhorn (Widenhorn, 2006) for an ideal reflection of velocity. At the top-right corner of e_y = 1 and e_x = 1, i.e. a collision on a “sticky" surface

with large dependence on ω_1 that conserves normal velocity after collision, permitted impact locations move towards colors (violet and red) closer to the goal line, except at large positive ω_1's. As a general trend, the very top planes of all columns demonstrate competing contributions by e_y and ω_1, where increasing e_y's restrict the range of reflected angles for all ω_1 and therefore tend to homogenize the plane colors.

In total, less than 2% of all trials produced double bounces. The above analysis demonstrates that double bounces are generally constrained to thin slices of impact areas on the first goal post, except at large positive values of e_x, i.e. “sticky" surfaces, where ω_1 plays a significant role in altering reflection angles. On such surfaces, a wider area of impact permits double bounces, but within constrained combinations of v_1 and ω_1.

For all successful double bounce trials, the distributions of impact locations for both the first and second bounces are illustrated in Figure (6). In agreement with Figure (5), the first bounce distributions are concentrated (indicated by dark shades) at angles in the vicinity of 30° (i.e. blue in Figure (4)). The histogram on the top-left showing the x-coordinate distributions of impact locations accordingly shows a peak at about 0.04 m from the center of the first post. By contrast, the second bounce impacts are distributed widely over the left-half (i.e. the side facing the first post) of the second post. This half of the second post receives the various reflected trajectories off the first post that are scattered over a wide range owing to the various coefficients of restitutions (e_x and e_y) and angular velocities (ω_1) involved, and subsequently produces the provided distribution.

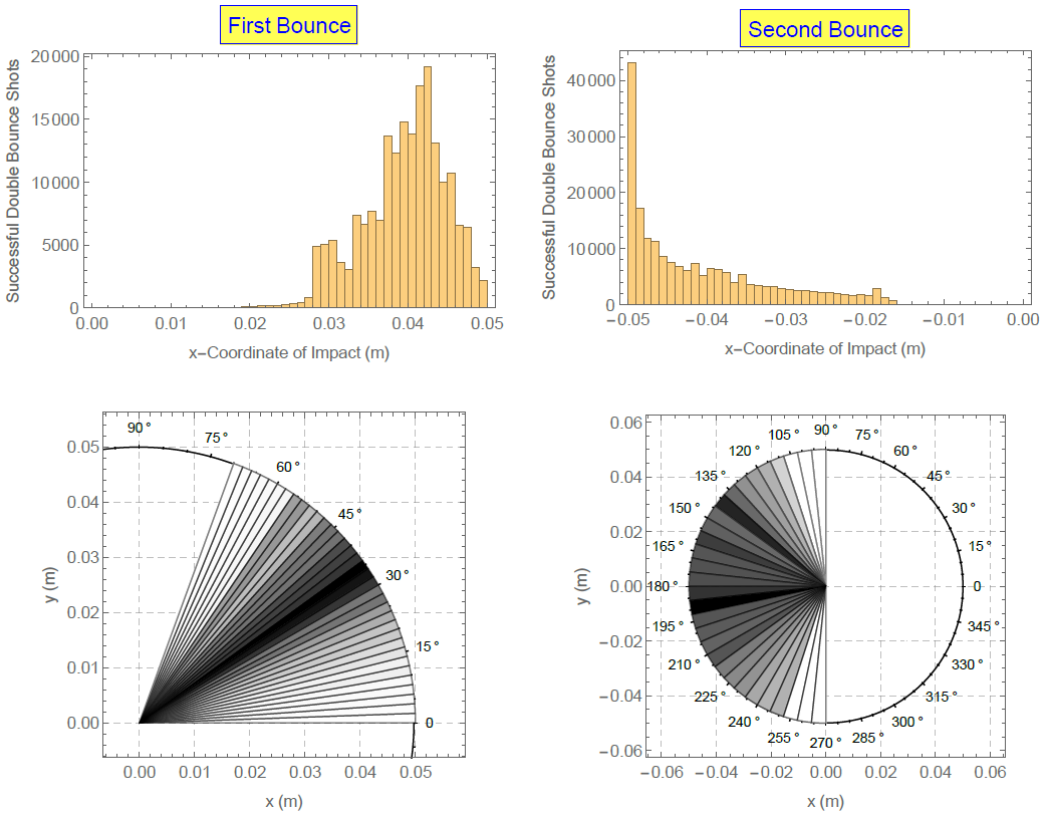

Figure 6. Distribution of impact locations of successful double bounce instances on the first post (left column) and second post (right column). The top row shows distributions ordered by x-coordinates of impact points (defining x = 0 at center of each post). For both posts, the +x-axis points from the center of the first post to the center of the second post (see Figure (2)). The bottom row shows distributions ordered by angular positions of impact on each post (defining the goal line as 0°) represented by grayscale intensity, where black represents maximum frequency and white represents zero frequency of data points.

The change in speeds and angular velocities for all successful double bounce trials before and after the first and second bounces are illustrated in Figure (7).

The first column shows that among all trials analyzed, positive ω_1 (i.e. a top-spin) is more likely than a negative ω_1 (i.e. a back-spin) to produce a double bounce, while it is almost equally likely with any v_1 (the last bar in the v_1 histogram is smaller owing to sampling termination at 45 m/s). After the bounces, ω_2 and ω_3 assume decaying forms extending up to 400 rad/s and 300 rad/s respectively, owing to friction upon impact as dictated by e_x. The rebound speeds v_2 and v_3 also assume a decaying form corresponding to energy re-distribution by impact.

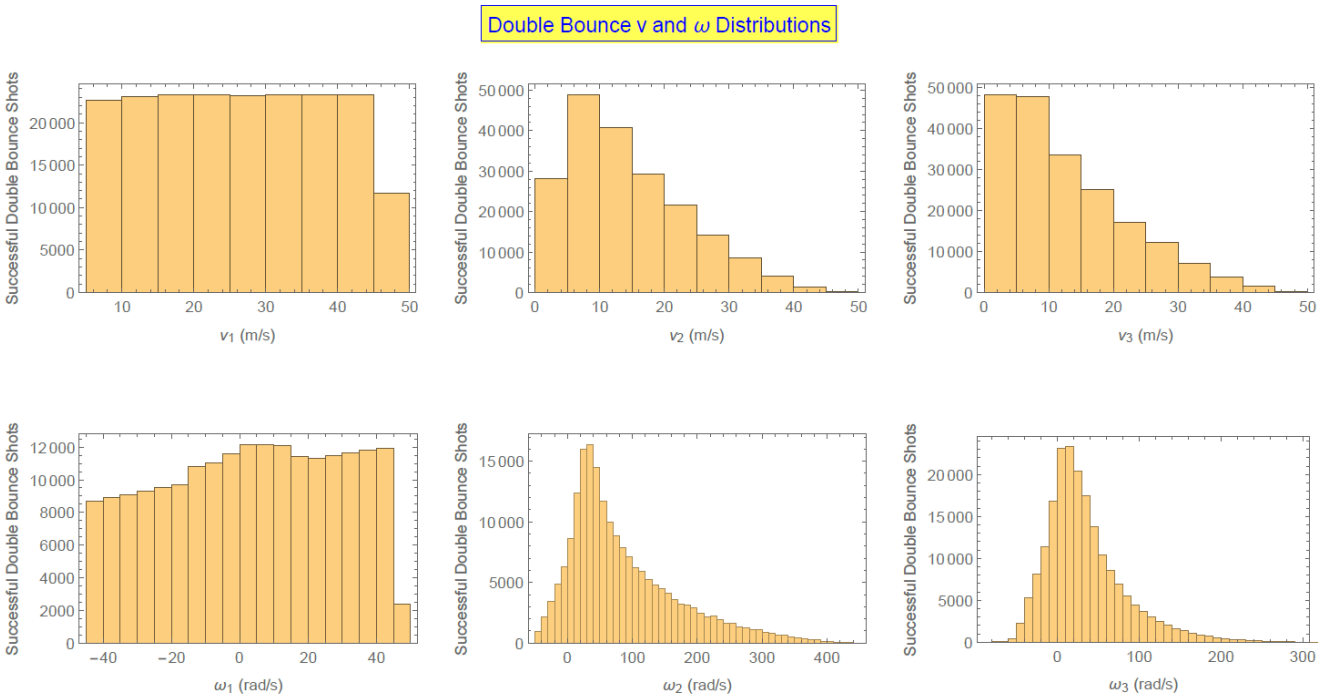

Figure 7. Distributions of speeds (v_1, v_2, v_3) and angular velocities (ω_1, ω_2, ω_3) for all successful double bounce instances. The left and middle columns refer to v_1, ω_1 and v_2, ω_2 before and after the first bounce respectively, whereas the right column represents v_3 and ω_3 after the second bounce. The first column shows that double bounces are more favored by positive ω_1's than negatives, but all v_1's are almost equally favored (the last bar in the v_1 histogram is smaller owing to sampling termination at 45 m/s). Also, it is observed that both (linear) speed and angular velocities assume a decaying form after impact.

As illustrated above in Figure (5), creating a double bounce from a penalty kick requires precise combinations of v_1 and ω_1 at narrow angular sectors of impact. The

criteria for triple bounces are even stricter, leading to a much smaller fraction of successful triple bounce trials, as described in the next section.

Triple Bounce

A sample successful triple bounce trajectory is shown in Figure (8).

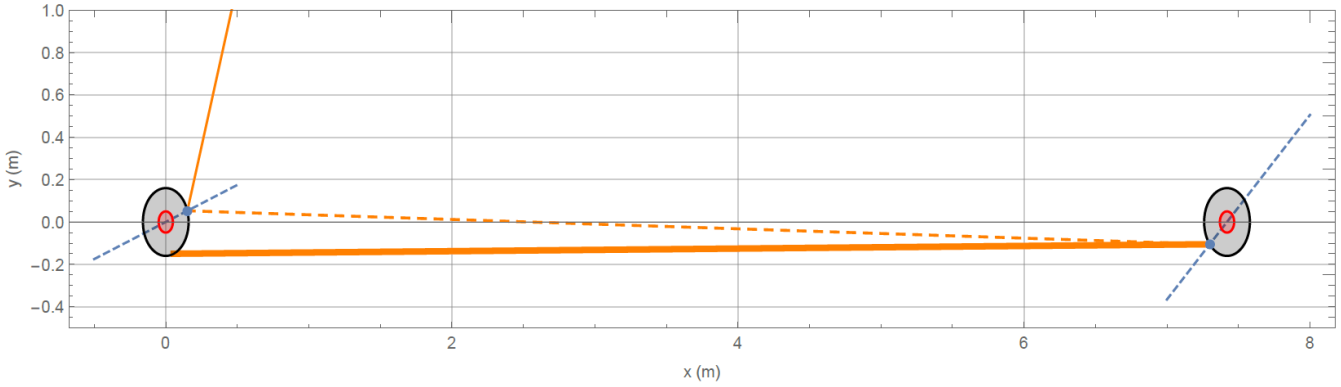

Figure 8. An example triple bounce trajectory drawn to scale showing the path of the ball from launch to third bounce. The first post is centered at the origin (0,0) m and the second post at (7.42,0) m. The dashed lines passing through these centers represent the normals at points of impact. The ball starts from the penalty spot above (not shown in figure) and strikes the first post (trajectory shown by thin, solid line), then follows the reflected trajectory after the first bounce from the first post to the lower part of the second post (dashed line) and finally is reflected back to the first post (thick, solid line) to complete the triple bounce.

Using the same color scheme as used for the previous section in Figure (4) and Figure (5), the successful triple bounce trials are presented according to their v_1, ω_1, e_x, e_y and impact locations for the first bounce in Figure (9).

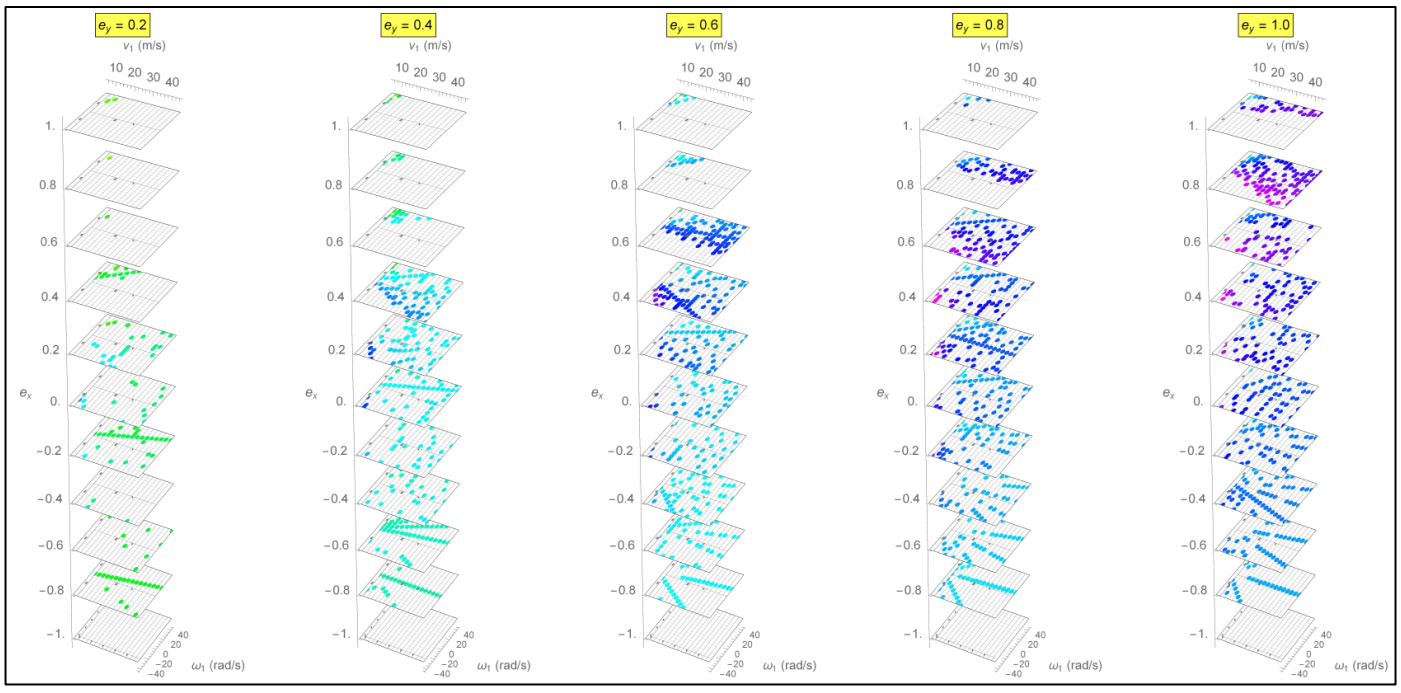

Figure 9. Representation of all data points that produce successful triple bounces categorized by e_y (columns), e_x (rows), v_1 (x-axis of planes) and ω_1 (y-axis of planes). Each successful triple bounce instance is assigned a color corresponding to the scheme described in Figure (4) to designate its impact point on the first goalpost during the first bounce (white dots indicate absence of triple bounce instances). Altogether, the first bounce impact location and the v_1, ω_1, e_y and e_x of every successful triple bounce are captured in this figure.

Since successful triple bounces form a subset of successful double bounces, Figure (9) consists of filtered data points from Figure (5). A tiny fraction of successful triple bounce trials appears at e_y = 0.2, and the corresponding fractions progressively increase with e_y. At the same time, the impact locations gradually shift from higher angles (green) to lower angles (blue and violet). The highest concentration appears at e_y= 1 and e_x = 0.8, and in general, higher concentrations of data points are observed between e_x = -0.8 and e_x = 0.8, indicating that goalposts having a certain amount of “stickiness" favor triple bounces.

The impact location distributions are shown in Figure (10).

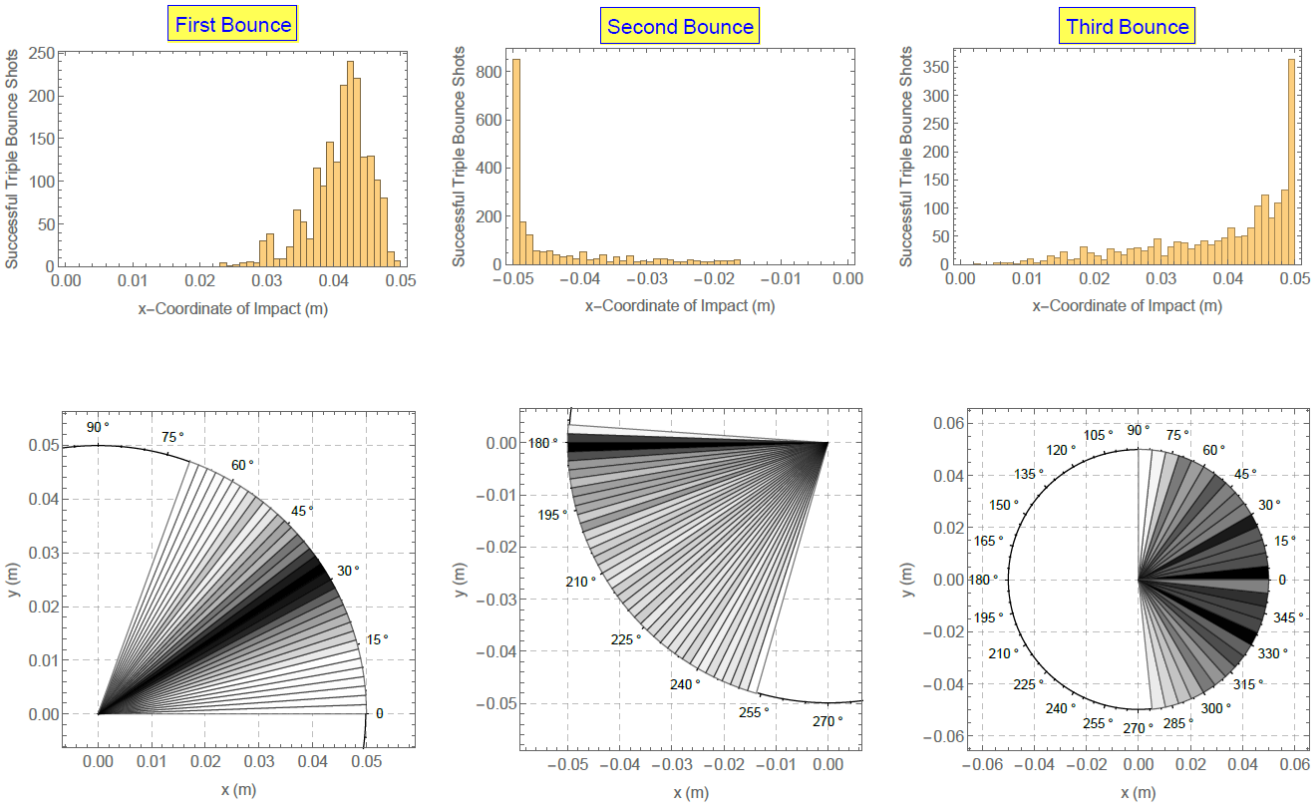

Figure 10. Distribution of impact locations of successful triple bounce instances for the first bounces (left column), the second bounces (middle column) and the third bounces (right column). The top row shows distributions ordered by x-coordinates of impact points (defining x = 0 at center of each post). For all posts, the +x-axis points from the center of the first post to the center of the second post (see Figure (2)). The bottom row shows distributions ordered by angular positions of impact points on each post (defining the goal line as 0°) represented by grayscale intensity, where black represents maximum frequency and white represents zero frequency. The first bounce distribution resembles the corresponding distribution for successful double bounces in Figure (6). In contrast, the second bounce distribution shows that triple

bounces are generated overwhelmingly by impacts below the y-axis, with a preference closer to the goal line at y = 0 (i.e. 180°). The third bounces are more uniformly distributed over the right-half of the first post that faces the second post.

Figure (10) shows that for successful triple bounces, the first bounce distribution mimics that of successful double bounces, with a peak at the same sector at approximately 30°. The second bounce distribution shows concentration at about 180°, i.e. the sector of the second post located on the goal line facing the first post. Also, no triple bounce is produced by any second bounce that occurs significantly above the goal line (i.e. 180°). The remaining triple bounces occur at impact locations below the y-axis, i.e. inside the goal. The third bounces are distributed over almost the entire right-half of the first post that faces the second post.

The second bounces that occur below the y-axis must carry large negative ω_2's that change the rebound trajectory back towards the first post. Figure (11) shows the distribution of ω_2 over second bounce impact locations, as well as the reflection angle ϕ_3 after the second bounce.

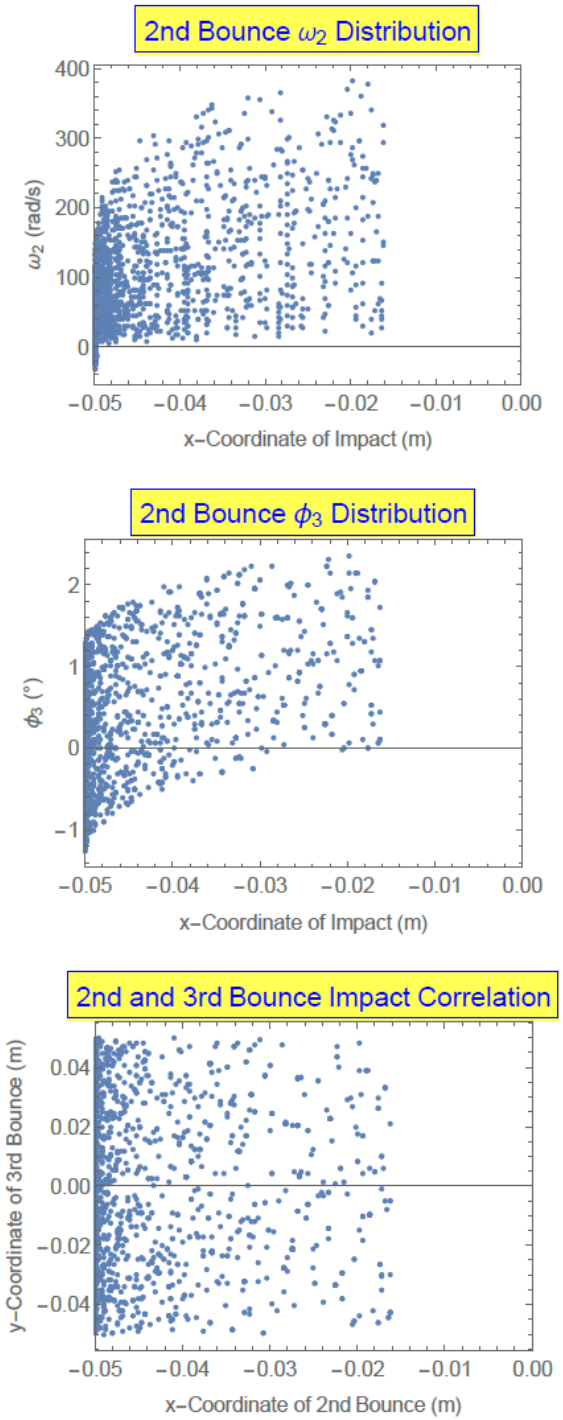

Figure 11. Scatter plots of ω_2 (top), _3 (middle) and y-coordinate of third bounce impact (bottom) as a function of the x-coordinate of second bounce impact for successful triple bounces, where x = 0 is defined at the center of the second post and the +x-axis points from the center of the first to the second post. For impacts closer to x = 0, the top diagram shows that larger ω_2, i.e. larger backspins, are required to rebound the ball back towards the first post, and the middle diagram shows that larger positive ϕ_3's are required to travel back to the first post since impacts take place below the y-axis (see Figure (10)). The bottom diagram shows that reflections from the second bounce scatter uniformly along the first post during third bounces.

As expected, for successful triple bounce trials where the second bounce occurs below the y-axis, i.e. x-coordinate closer to 0, ω_2 is seen to assume large values. Although positive values of ω_2 are plotted, the resulting collision with the second goalpost below the y-axis effectively produces a negative ω_2, i.e. a backspin (see Figure (3) and Eq. (21)). Similarly, the larger positive ϕ_3 are observed for the same trials as above, indicating that the reflected trajectories travel upwards towards the positive y-axis, i.e. on the same side of the normal as the incident trajectory, as a result of the backspins. The plot of second bounce x-coordinates and third bounce y-coordinates at the bottom of Figure (11) shows that there is no significant correlation between the impact points of second and third bounces, as illustrated by the relatively uniform scattering of data points above ($y_{B_3} \geq 0$) and below ($y_{B_3} \geq 0$) the goal line (y = 0) at any x-coordinate of impact, in agreement with the third bounce distributions depicted in Figure (10).

As with Figure (7), the change in speeds and angular speeds before and after the first and second bounces are illustrated in Figure (12) for all successful triple bounce trials. Apart from a greater emphasis on positive ω_1's over negative ω_1's, the observed distributions closely resemble Figure (7), and indicate that successful triple bounces form an uniform subset of double bounces with respect to speeds and angular velocities.

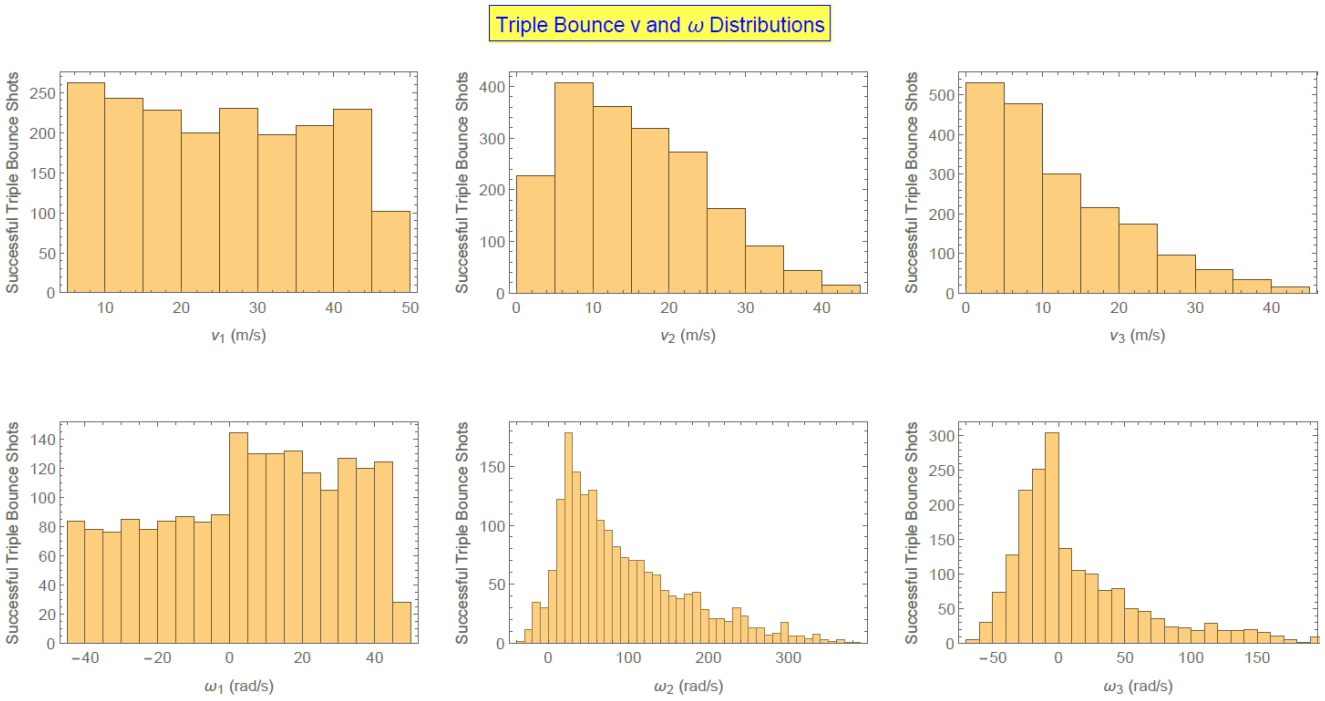

Figure 12. Distributions of speeds (v_1, v_2, v_3) and angular velocities (ω_1, ω_2, ω_3) for all successful triple bounce instances. The left and middle columns refer to v_1, ω_1 and v_2, ω_2 before and after the first bounce respectively, whereas the right column represents v_3 and ω_3 after the second bounce. The first column shows that triple bounces are more favored by positive ω_1's and slightly more favored by small v_1's. Also, it is observed that both (linear) speed and angular velocities assume a decaying form after impact.

Before we conclude this section, it ought to be pointed out that triple bounces under specified conditions require impacts at very narrow slices of the first goal post during their first bounces. In this study, while fine angular spacing has been employed, it is possible that some of these triple bounces have been missed owing to inadequate resolution.

CONCLUSION

By simulating soccer balls travelling on a plane with specified linear and angular velocities from the penalty spot to one of the goalposts, and calculating rebound trajectories for one or more collisions with both goalposts, we generated a large dataset spanning several variables (v_1, ω_1, ϕ_1, e_x, e_y) and used it to identify instances of double and triple bounces.

The results show that for any specified set of variables, double and triple bounces occur from penalty kicks that strike specific narrow slices (<2°) of the first goalpost, corresponding to rarity of such events in real life. In the case of “sticky" goalpost surfaces characterized by large e_x values that reduce the reflection angle, there is greater dependence on ball speed and spin, and the slices of the first goalpost that can facilitate multiple bounces tend to become wider. For surfaces characterized by large e_y values that conserve normal velocity component, these goalpost slices tend to shift closer to the goal line. Since triple bounces form a subset of double bounces, they require narrower impact slices during the first bounce, and are found to be increasingly favored by larger e_y values and by e_x values in the range of $-0.8 \leq e_x \leq 0.8$.

Among all trials, double and triple bounces are found to be more favored by positive ω_1's and at angular impact locations of about 30° on the first bounce. A triple bounce can only be generated if the second bounce impact occurs below the y-axis or at the goal line. Subsequently, triple bounces are overwhelmingly more favored by positive ω_2's that generate back-spins upon impact below the y-axis. Altogether, less than 2% of all trials produced double bounces, and less than 1% of successful double bounce trials produced triple bounces.

Although actual parameters e_y and e_x for a real-life goalpost and soccer ball are not available (estimated guess by Dr. Cross via private communication: $e_y = 0.7$ and $e_x = 0.2$), this paper covers a wide range of possible combinations that produce noticeably different results regarding double and triple bounces. Upon making experimental measurements of e_y and e_x, comparison with the appropriate subspaces of the simulated data can yield insight to double and triple bounce behavior of a real system.

In the double bounce penalty kick that occurred in the 2015 MLS match referred in the introduction, it is observed in the video that the ball struck the first post with a topspin at about the 45° sector or higher. In addition, the ball strikes this first post ≈ 1 ft above the ground. The rebounding ball bounces on the ground before striking the second post at a large angle (> 45°) measured from the goal line (as defined in Fig. (4)) and finally travels away from the goal. According to Figure (5), it would require e_y to be unrealistically small (e_y ≈0.2) for a double bounce to occur at this first post impact

location. However, the path of the ball from one post to the other is not linear and is slightly (≈ 1 cm) longer than assumed in this simulation. Furthermore, upon bouncing on the ground, the rebounding ball could have deviated slightly towards the second post. These slight deviations can possibly account for the discrepancy between simulation and observation results.

REFERENCES

Brody, H. 1984. That's How the Ball Bounces. The Physics Teacher, 22, 494-497 (1984).

Cross, R. 2002. Grip-slip Behavior of a Bouncing Ball. Am. J. Phys. 70(11), 1093-1102 (2002).

Cross, R. 2002. Measurements of the Horizontal Coefficient of Restitution for a Superball and Tennis Ball. Am. J. Phys. 70(5), 482-489.

Cross, R. 2005. Bounce of a Spinning Ball Near Normal Incidence. Am. J. Phys. 73(10), 914-920.

Elkin, J. 1965. A Deceptively Easy Problem. The Mathematics Teacher, 58(3), 194-199.

Laws of the Game. 2019-2020. https://www.fifplay.com/downloads/documents/laws-of-the-game-2019-2020.pdf.

Widenhorn, R. 2016. Hitting the Goalpost: Calculating the Fine Line Between Winning and Losing a Penalty Shootout. The Physics Teacher, 54(7), 434-438.

Wolram Mathematica. 2021. https://www.wolfram.com/mathematica.

APPENDIX

Angular Velocity Sign Convention

The sign of the angular velocity ω is based on the concepts of topspin and backspin when a rotating ball strikes a surface. If the axis of rotation of the ball is normal to the plane defined by v_x and v_y, then the sign of ω is determined by the direction of v_x and the direction of motion of the point on the ball that strikes the surface. At the instant before impact, if the direction of this point is opposite to v_x, the ball is said to possess topspin and ω is considered to be positive. If the direction of this point is the same as v_x, the ball is said to possess backspin and ω is considered to be negative (Figure (13)).

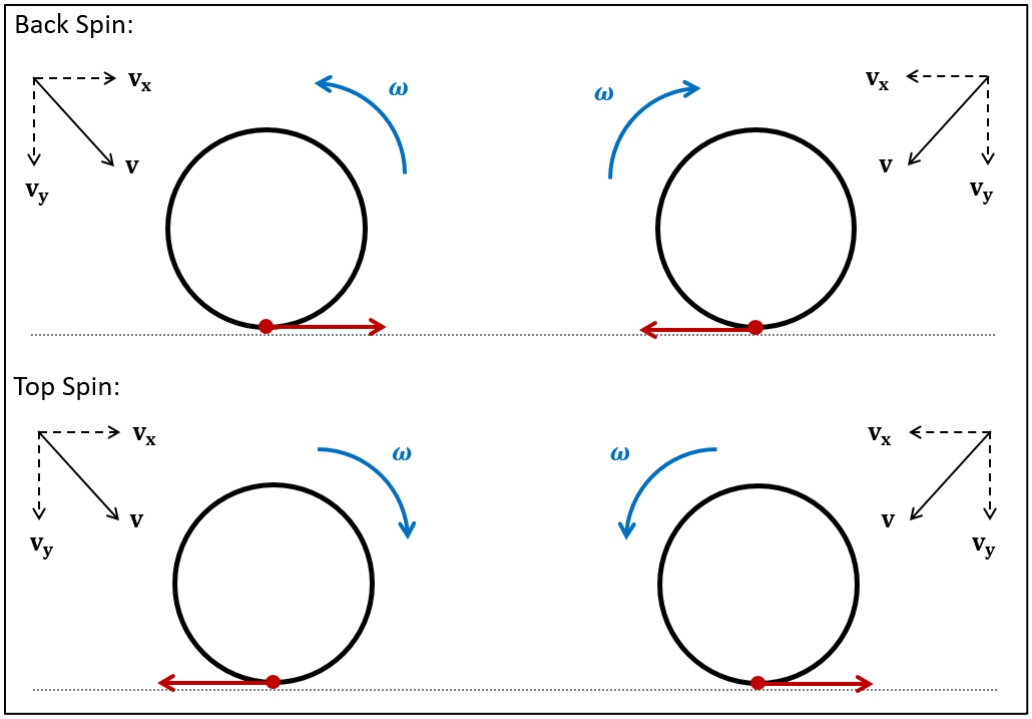

Figure 13. *Top Row:* Back spin for a ball rotating counterclockwise (left) and clockwise (right). The red arrow shows the velocity of the point on the ball that is about to strike the surface. This velocity points in the same direction as v_x in both cases. *Bottom Row:* Top spin for a ball rotating clockwise (left) and counterclockwise (right). The red arrow shows the velocity of the point on the ball that is about to strike the surface. This velocity points opposite to v_x in both cases.

Deriving θ_1 and ϕ_2

For the goalpost centered at (x_{P_1}, y_{P_1}), the normal to the point (x_{B_1}, y_{B_1}) where the ball strikes the post makes an angle of θ_N with the x-axis (see Figure (14)):

$$\theta_N = \arctan\left(-\frac{\sqrt{(R_{ball}+R_{post})^2-(x_{B_1}-x_{P_1})^2}}{x_{P_1}-x_{B_1}}\right) \qquad (26)$$

within the range $-90° < \theta_N \leq 90°$. Also, the angle θ_x between the first bounce reflected trajectory and the normal is calculated by:

$$\theta_x = \arctan\left(\frac{v_{xf_1}}{v_2}\right) \qquad (27)$$

where v_2 is the rebound speed and v_{xf_1} is the tangential component of the rebound velocity.

Representing these angles in Figure (14), it is observed that geometrically $\theta_1 = \phi_1 - \theta_N$ and $\phi_2 = \theta_x - \theta_N$, where a negative sign is placed before each θ_N to compensate for the negative angle generated by the negative slope.

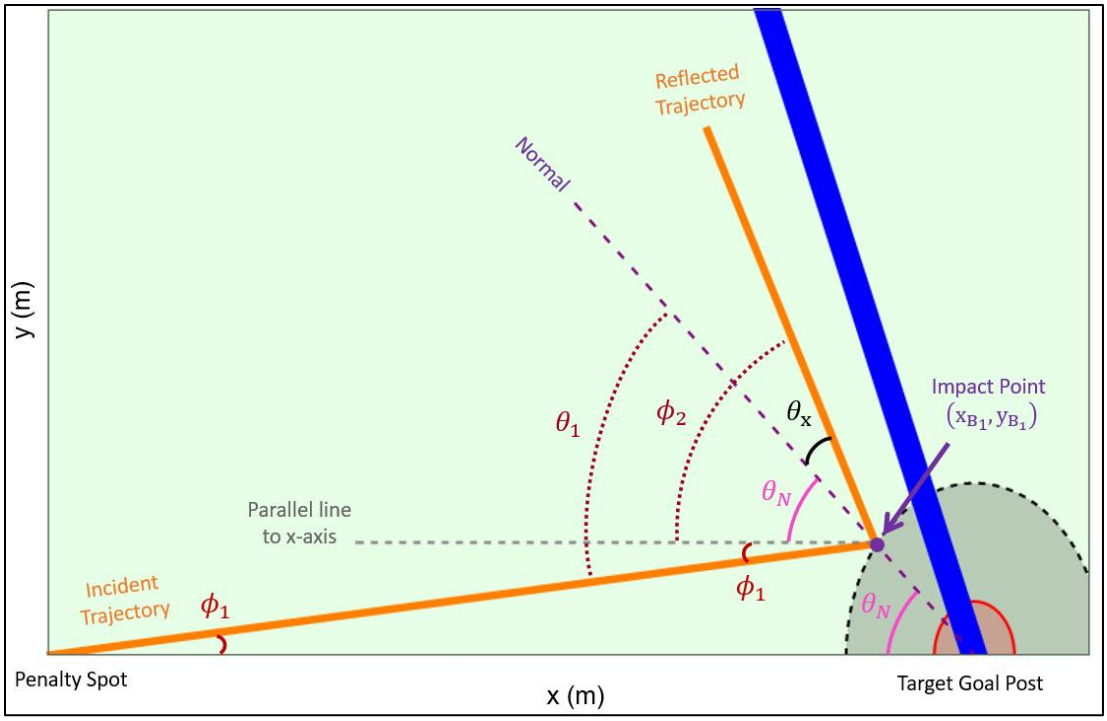

Figure 14. Illustration of the angles ϕ_1, θ_1, ϕ_2, θ_N and θ_x for the first bounce. The two ϕ_1 angles are alternate angles and the two θ_N angles are corresponding angles. It is observed that $\theta_1 = \phi_1 - \theta_N$ and $\phi_2 = \theta_x - \theta_N$ (where the negative signs compensate for negative values of θ_N).